THE JOURNAL OF BIOLOGICAL CHEMISTRY VOL. 285, NO. 41, pp. 31661–31671, October 8, 2010

Polarization and Migration of Hematopoietic Stem and Progenitor Cells Rely on the RhoA/ROCK I Pathway and an Active Reorganization of the Microtubule Network[S]

Received for publication, May 14, 2010, and in revised form, August 1, 2010 Published, JBC Papers in Press, August 3, 2010, DOI 10.1074/jbc.M110.145037

Ana-Violeta Fonseca[‡], Daniel Freund[‡], Martin Bornhäuser[§¶1], and Denis Corbeil[‡§2]

From the [‡]Tissue Engineering Laboratories, Technische Universität, the [§]Deutsche Forschungsgemeinschaft Research Center and Cluster of Excellence for Regenerative Therapies, Technische Universität, and the [¶]Medical Clinic and Polyclinic I, University Hospital, D-01307 Dresden, Germany

Understanding the physiological migration of hematopoietic progenitors is important, not only for basic stem cell research, but also in view of their therapeutic relevance. Here, we investigated the role of the Rho kinase pathway in the morphology and migration of hematopoietic progenitors using an *ex vivo* co-culture consisting of human primary CD34$^+$ progenitors and mesenchymal stromal cells. The addition of the Rho kinase inhibitor Y-27632 led to the abolishment of the uropod and microvillar-like structures of hematopoietic progenitors, concomitant with a redistribution of proteins found therein (prominin-1 and ezrin). Y-27632-treated cells displayed a deficiency in migration. Time-lapse video microscopy revealed impairment of the rear pole retraction. Interestingly, the knockdown of ROCK I, but not ROCK II, using RNA interference (RNAi) was sufficient to cause the referred morphological and migrational changes. Unexpectedly, the addition of nocodazole to either Y-27632- or ROCK I RNAi-treated cells could restore their polarized morphology and migration suggesting an active role for the microtubule network in tail retraction. Finally, we could demonstrate using RNAi that RhoA, the upstream regulator of ROCK, is involved in these processes. Collectively, our data provide new insights regarding the role of RhoA/ROCK I and the microtubules in the migration of stem cells.

The transplantation of hematopoietic stem and progenitor cells (HSPCs)[3] is an established procedure for treating hematological diseases. But still, many aspects of HSPC homing and engraftment after transplantation are not fully understood. Having the capacity to self-renew and to differentiate, engrafted HSPCs can replenish the hematopoietic system upon the appropriate stimuli provided by the bone marrow-supportive stroma. Cell migration plays a fundamental role in this process, because HSPCs need to reach their appropriate niche within the bone marrow cavity (1).

An important prerequisite for HSPC migration is the acquisition of a polarized morphology through the reorganization of the cytoskeleton elements leading to the formation of a lamellipodium at the front side and a uropod at the rear (2). The posterior protrusion is a unique structure common to HSPCs and lymphocytes (2, 3), which is thought to be an important adhesive element and to function as an anchor point for recruiting other cells (4–6). In both cell types, the uropod concentrates several adhesion molecules such as intercellular adhesion molecule-1/3 and P-selectin glycoprotein ligand-1 (PSGL-1) (2, 6, 7). The cholesterol-interacting membrane protein prominin-1 (CD133) is concentrated therein as well (2). The asymmetric distribution of HSPC membrane components may involve cholesterol-based membrane microdomains (lipid rafts) (8, 9). Members of the actin-binding ezrin/radixin/moesin (ERM) protein family notably ezrin may participate in the formation and/or stabilization of the uropod as demonstrated using a lymphoma cell line (10). These cytoplasmic adaptor proteins may anchor certain uropod-associated membrane proteins to the cortical actin cytoskeleton (11).

The Rho family of GTPases was found to govern various mechanisms modulating cytoskeletal dynamics and therefore cell migration (12). Three of them, *i.e.* Rho, Rac, and Cdc42, were extensively studied in fibroblasts, and their functions were unraveled. For instance, Rho regulates the assembly of actin/myosin stress fibers and the formation of focal contacts (13), whereas Rac and Cdc42 are involved in the formation of lamellipodia/membrane ruffles and filopodia, respectively (14, 15). Although some reports implicate RhoA on the regulation of lamellae formation and membrane ruffling in epithelial cells (16, 17), in leukocytes it appears to exert its effects mainly at the rear of migrating cells (18, 19). Therein RhoA is required for tail retraction through its effector protein Rho-associated coiled-coil protein kinase (ROCK). The latter was also found to be important for the maintenance of the uropod (10). Two ROCK genes have been described, *ROCK I* and *II* (20–23). In fibroblasts ROCK I seems to be important for the formation of stress fibers, whereas ROCK II acts as a counterbalance in regulating the microfilament bundle and focal adhesion site (24). Their physiological relevance in HSPCs is unknown.

In the present study, we address the potential implication of the Rho kinase pathway in the polarization and migration of

[S] The on-line version of this article (available at http://www.jbc.org) contains supplemental videos S1–S4 and Figs. S1–S3.

[1] Supported by the Deutsche Forschungsgemeinschaft (DFG Grant SFB 655 B2).

[2] Supported by the DFG (Grants SFB/TR83 #6 and SFB 655 B3). To whom correspondence should be addressed: Tissue Engineering Laboratories, Technische Universität Dresden, Tatzberg 47–49, D-01307 Dresden, Germany. Tel.: 49-351-463-40118; Fax: 49-351-463-40244; E-mail: corbeil@biotec.tu-dresden.de.

[3] The abbreviations used are: HSPC, hematopoietic stem and progenitor cell; ERM, ezrin/radixin/moesin; MSC, multipotent mesenchymal stromal cell; ROCK, Rho-associated coiled-coil protein kinase; RNAi, RNA interference; SDF-1α, stromal cell-derived factor-1α.

human HSPCs by means of a co-culture system where primary multipotent mesenchymal stromal cells (MSCs) are used as feeder cell layer (25). Our findings based on the use of a synthetic inhibitor and RNAi experiments show that either the inhibition or knockdown of Rho kinases, particularly ROCK I, results in the loss of a polarized morphology and in a migration deficiency.

EXPERIMENTAL PROCEDURES

Antibodies—Goat and rabbit polyclonal antibodies directed against ROCK I and II, respectively, and the mouse anti-RhoA monoclonal antibody (mAb) were purchased from Santa Cruz Biotechnology, Inc. (#sc-6056, sc-5561, and sc-418, respectively; Santa Cruz, CA). Mouse anti-ezrin and anti-PSGL-1 mAbs were obtained from Acris Antibodies (#DM380, Hiddenhausen, Germany) and BD Biosciences (#556053, Heidelberg, Germany), respectively, and the rat anti-α-tubulin mAb from Serotec (clone MCA78S, Oxford, UK). mAb against human prominin-1 was purchased from Miltenyi Biotec (clone CD133/1, #130-090-422, Bergisch Gladbach, Germany). Secondary Cy™3-conjugated goat anti-mouse IgG and Cy™2-conjugated goat anti-rat IgG were purchased from Jackson ImmunoResearch Laboratories (#115-165-146 and 112-225-167, Soham, UK). Secondary HRP-conjugated goat anti-rabbit IgG, goat anti-rat IgG and rabbit anti-mouse IgG were obtained from Jackson ImmunoResearch Laboratories (#111-035-144, 112-035-167, and 315-035-045). Secondary HRP-conjugated rabbit anti-goat Ig was purchased from Dako (#P0449, Hamburg, Germany).

Reagents—The ROCK inhibitor Y-27632 and latrunculin B were provided by Calbiochem (#688001 and 428020, Merck GmbH, Darmstadt, Germany). Nocodazole and 4,6-diamidino-2-phenylindole (DAPI) were purchased from Sigma-Aldrich (#M1404 and 32670, St. Louis, MO). ROCK I and II, RhoA, and negative control (low GC content) Stealth siRNA oligonucleotides were purchased from Invitrogen (oligonucleotide IDs: HSS109291, HSS114108, HSS100655, and 12935–200, respectively, Karlsruhe, Germany). Alexa Fluor® 635-conjugated Phalloidin was purchased from Molecular Probes (#A34054, Eugene, OR).

HSPC Isolation, siRNA Transfection, and Co-cultivation with MSCs—Mobilized peripheral blood from healthy donors was collected after informed consent and approval by the institutional review board. Granulocyte colony-stimulating factor-mediated mobilization was achieved as described previously (25). $CD34^+$ HSPCs were immunoisolated directly after leukapheresis by immunomagnetic separation using the MACS system (Miltenyi Biotec). Briefly, cells were washed with MACS buffer (PBS containing 2 mM EDTA and 0.5% human serum albumin (Baxter Deutschland GmbH, Germany)) and incubated with blocking agent and anti-CD34 beads for 30 min at 4 °C. After washing with MACS buffer, the cell pellet was resuspended in 1 ml of the same buffer and applied to an LS-column, previously placed into a magnetic field, followed by two washing steps with 5 ml of MACS buffer each. Cells retained in the LS-column were eluted by taking the column out of the magnet and flushing with 5 ml of MACS buffer.

$CD34^+$-enriched HSPCs were resuspended in serum-free medium (Cell Gro SCGM, CellGenix, Freiburg, Germany) containing 50 ng/ml stem cell factor, 50 ng/ml FLT3-L (CellGenix) and 15 ng/ml IL-3 (R&D Systems, Mannheim, Germany) (HSPC complete medium), counted and either plated immediately on MSCs (see below) at a density of 10^4 HSPCs per milliliter of medium and cultured for 3 or 7 days at 37 °C in a 5% CO_2 atmosphere as described (25), or transfected by electroporation with 1 μg of siRNA per 10^6 cells using the human CD34 cell Nucleofector kit according to the manufacturer's instructions (#VPA-1003, Amaxa AG, Cologne, Germany). After the transfection, HSPCs were washed in serum-free medium and spun down, and the cell pellets were incubated for 15 min at 37 °C and 5% CO_2 as described (26). Transfected HSPCs were then distributed onto the MSC monolayer at a density of $15–30 \times 10^4$ HSPCs per milliliter of medium and cultured for 2 days. Under these conditions the reduction of a given protein was observed in >90% of the cells by immunofluorescence and/or FACS (data not shown).

Bone marrow aspirates were collected from healthy donors after informed consent and approval of the institutional review board. MSCs were isolated according to modifications of previously reported methods (27) (for technical details see Ref. 25). The isolated primary cells were seeded into 75-cm^2 flasks containing MSC medium, consisting of Dulbecco's modified Eagle's medium (DMEM), low glucose, supplemented with 1% L-glutamine (Invitrogen) and 10% fetal calf serum (FCS, PAA Laboratories, Pasching, Austria). MSC cultures were grown at 37 °C under a humidified 5% CO_2 atmosphere. Non-adherent cells were removed after 24 h by washing with PBS-human serum albumin solution. The medium was subsequently changed every 4 days and after 2 weeks, the cultures were 90% confluent. MSCs were recovered using Trypsin-EDTA (Invitrogen) and replated at a density of $5–6 \times 10^3$ cells per cm^2 of surface area, as passage 1 (P1) cells. The cells were used up to five passages. P1–P5 cells were routinely checked by flow cytometry for the presence of the characteristic cell surface molecules CD73, CD90, CD105, and CD166, and the absence of CD45 and CD34 as described (28).

Drug Treatments—For treatment of HSPCs with Y-27632, an aqueous solution of the reagent was added to the freshly isolated HSPCs, after plating them on MSCs, at a final concentration of 10 μM. Cells were cultured in the presence or absence of Y-27632 for 3 or 7 days. In the case of the siRNA transfection experiments, cells were cultured with Y-27632 for 2 days. Both latrunculin B and nocodazole were dissolved in DMSO and added to HSPCs 3 days after culture on MSCs, at a final concentration of 5 μM and 1 μM, respectively. Cells were incubated for 30 min. Alternatively, nocodazole was added to the siRNA-transfected HSPCs 2 days after transfection.

Immunofluorescence—HSPCs co-cultured for 3 days on MSCs growing on fibronectin-coated glass coverslips were gently washed with PBS and fixed with 4% paraformaldehyde in PBS for 30 min at room temperature. Coverslips were then rinsed with PBS and incubated in 50 mM ammonium chloride for 10 min at room temperature. Fixed cells were permeabilized and blocked with 0.2% saponin and 2% FCS in PBS (blocking solution) for 30 min at room temperature. Cells were incubated

sequentially for 30 min at room temperature with either anti-prominin-1 mAb (1:50) or anti-ezrin mAb (1:20) or anti-PSGL-1 mAb (1:50) followed by Cy™3-conjugated goat anti-mouse IgG secondary antibody (1:500), all diluted in the blocking solution. For the actin and α-tubulin double-labeling, fixed and permeabilized cells were incubated with anti-α-tubulin mAb (1:100) followed by Cy™2-conjugated goat anti-rat IgG secondary antibody (1:500) mixed with Alexa Fluor 635-conjugated Phalloidin (1:200). Nuclei were labeled with 1 μg/ml of either DAPI (Molecular Probes) or Hoechst 33258 (Invitrogen). Alternatively, living cells were cell surface-labeled with anti-prominin-1 mAb in PBS containing 10% FCS, 1 mM $CaCl_2$, and 0.5 mM $MgCl_2$ for 30 min at 4 °C prior to paraformaldehyde fixation as described previously (29). Coverslips were rinsed sequentially with blocking solution, PBS, and distilled water, and mounted in Mowiol 4.88 (Calbiochem). The labeling of siRNA-transfected HSPCs was performed 48 h after the transfection. Labeled cells were observed with either a Zeiss LSM 510 Meta inverted or a Leica SP5 upright confocal microscope. The images shown were prepared from the confocal data files using Adobe Photoshop® and Illustrator®.

Immunoblotting—Detergent cell lysates were prepared 48 h after the HSPC transfection using RIPA buffer (1% Nonidet P-40, 0.5% sodium deoxycholate, 0.1% SDS, 0.15 M NaCl, 0.05 M Tris, pH 8.0) supplemented with a mixture of protease inhibitors (Roche Applied Science, Mannheim, Germany). Proteins were analyzed by SDS-PAGE and transferred to Immobilon PVDF membranes (pore size, 0.45 μm; Millipore Corp., Belford, MA) by standard procedures (30). After transfer, PVDF membranes were incubated for 1 h in blocking buffer (5% (w/v) low fat milk powder in PBS containing 0.3% Tween 20). The incubation with the primary antibodies (ROCK I, 1:200; ROCK II, 1:800; RhoA, 1:200; α-tubulin, 1:500) was performed overnight at 4 °C. In all cases, antigen-antibody complexes were visualized using horseradish-peroxidase-conjugated secondary antibodies followed by enhanced chemiluminescence (ECL System, Amersham Biosciences). For the detection of ROCK II, ROCK I was stripped from the PVDF membrane by shaking the membrane in 0.2 M NaOH for 30 min at room temperature followed by a washing step in distilled water. The membrane was then processed as described above.

Time-lapse Video Microscopy—Freshly isolated HSPCs were cultured for 3 days on MSCs grown on 24 × 60 mm fibronectin-coated coverslips, attached to a silicone reusable chamber. During the time-lapse recording, cells were kept in a 37 °C chamber with a 5% CO_2 atmosphere. Serial phase-contrast images were captured with an inverted microscope (Zeiss Axiovert 200M, 20× objective) at 30-s intervals. The images were built into a movie using the Metamorph software. Transfected HSPCs were imaged 48 h after the transfection. The tracking of HSPCs was done manually.

Scanning Electron Microscopy—Samples for the scanning electron microscopy analysis were prepared as previously described (25). Briefly, the co-cultured cells growing for 1 week on fibronectin-coated coverslips were fixed in 2% glutaraldehyde for 1 h at room temperature and then overnight at 4 °C. After being subjected to dehydration in an acetone gradient (30–100%), cells were critical point-dried in a CO_2 system (Critical Point Dryer CPD 030, BAL-TEC GmbH, Witten, Germany). Samples were then sputter-coated with gold (Sputter Coating Device SCD 050, BAL-TEC GmbH) and examined at 10-kV accelerating voltage in an environmental scanning electron microscope (XL 30 ESEM FEG, Philips, Eindhoven, The Netherlands).

Transwell Migration Assay—25×10^4 freshly isolated HSPCs resuspended in HSPC complete medium were incubated with or without 10 μM Y-27632 for 1 h at 37 °C. Half of the Y-27632-treated HSPCs were then incubated with 1 μM nocodazole for 30 min, after which 100 μl of cell suspension (12.5×10^4 cells) was added to the upper chamber of a 5-μm pore-sized polycarbonate Transwell (Corning Costar Corp., New York, NY). In the lower chamber, 600 μl of HSPC complete medium with or without 10 μM Y-27632 and/or 100 ng/ml stromal cell-derived factor-1 α (SDF-1α, Strathmann GmbH & Co. KG, Hamburg, Germany) were added to an MSC monolayer. After incubation for 1 h at 37 °C under a 5% CO_2 atmosphere, HSPCs in the upper and lower chambers were collected and counted. All assays were performed with HSPCs from three distinct donors, each of them in duplicate.

RESULTS

The Rho Kinase Pathway Is Involved in the Formation and/or Stabilization of Uropod and Microvillar-like Structures of Hematopoietic Progenitors—Primary human HSPCs have been described to have various morphologies upon cultivation on MSCs (25). They can be either spherical (Fig. 1*A*, *outlined arrowhead*) or polarized (Fig. 1*A*, *asterisk*) with the formation of distinct types of plasma membrane protrusion, *e.g.* uropod (Fig. 1*C*, *outlined arrow*), lamellipodium (Fig. 1, *C* and *E*, *filled arrow*). The presence of a uropod and lamellipodium at the rear and front pole, respectively, is a typical morphology of a migrating HSPC (Fig. 1*C*, supplemental video S1; see also Refs. 2, 25). The number of cells exhibiting a given morphology is conditioned by the culture time. For instance, ≈40% of HSPCs displayed a migrating morphology within the first 4 days, whereas this percentage decreased to 10–15% after 8 days (see supplemental Fig. S1).

Interestingly, the integrity of these plasma membrane protrusions appeared dependent on the Rho kinase pathway, because the incubation of HSPCs with Rho kinase inhibitor Y-27632 resulted in a dramatic alteration of the referred morphologies. Y-27632-treated cells displayed either a spherical (Fig. 1*B*, *outlined arrowhead*) or an elongated morphology (Fig. 1*B*, *filled arrowhead*). In the latter case, one to three long and thin plasma membrane protrusions could be observed (Fig. 1*B*). Upon incubation of cells with Y-27632 (*e.g.* for 3 or 7 days) <3% displayed a uropod ($n = 200$; data not shown), which is in agreement with a previous observation in lymphoma cells treated with the same inhibitor and under similar conditions (10). Furthermore, the lamellipodium of Y-27632-treated HSPCs appeared narrowed and to be preferentially formed at the tip of thin protrusions (Fig. 1, *D* and *F*, *arrow*) rather than close to the cell body, as in control cells (Fig. 1, *C* and E, *filled arrow*). In cells with spherical morphology, numerous microvillar-like structures are observed on the surface (Fig. 1*G*). Upon Y-27632 incubation, they become shorter and sparse (Fig. 1*H*). These latter

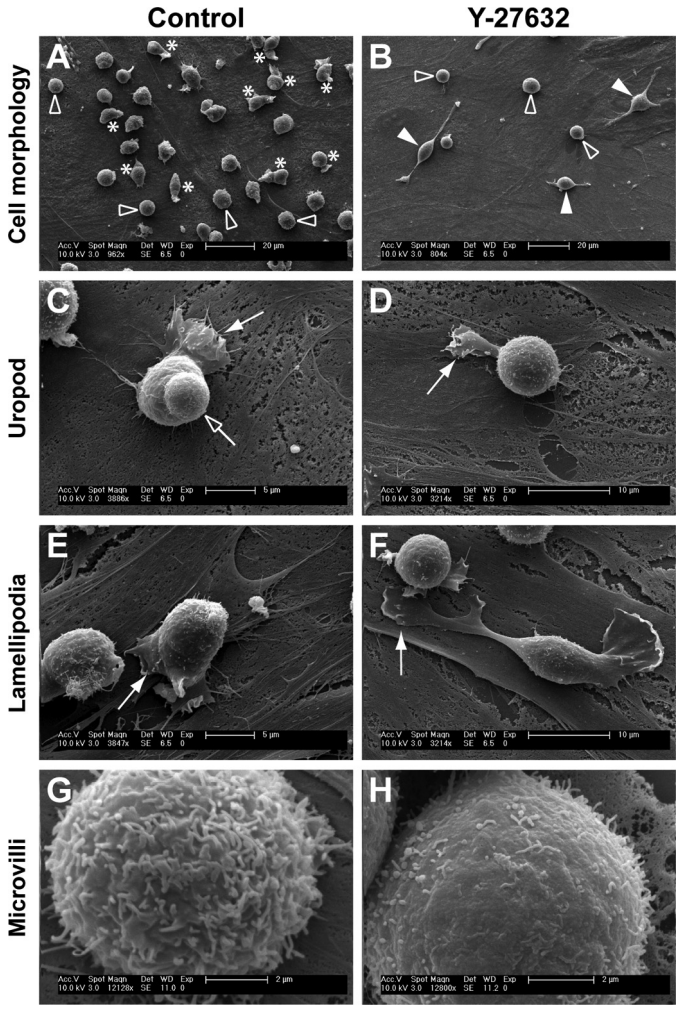

FIGURE 1. **ROCK inhibitor Y-27632 alters the morphology of hematopoietic progenitors.** HSPCs cultured on MSCs for 7 days in the absence (*A*, *C*, *E*, and *G*) or presence (*B*, *D*, *F*, and *H*) of Y-27632 were analyzed by scanning electron microscopy. *A* and *B*, untreated HSPCs (*Control*) can either be spherical (*outlined arrowhead*) or polarized (*asterisk*) with a uropod and/or lamellipodium (*A*), whereas Y-27632-treated HSPCs are mostly round (*outlined arrowhead*) or have one to three long and thin plasma membrane protrusions (*filled arrowhead*) (*B*). *C–F*, polarized HSPCs exhibit a uropod at the rear pole (*C*, *outlined arrow*), whereas most Y-27632-treated HSPCs do not (*D*). Y-27632-treated HSPCs have a narrower lamellipodium (*D*, *filled arrow*) in comparison to untreated cells (*C* and *E*, *filled arrow*). Large lamellipodia at the edge of thin protrusions are often observed in Y-27632-treated HSPCs (*F*, *filled arrow*). *G* and *H*, the surface of rounded HSPCs exhibits numerous microvillar-like structures (*G*) that are sensitive to the ROCK inhibitor (*H*).

observations appear nevertheless to vary with the donor (n = 4). These donor-related variations were not valid in the case of the lack of uropod and altered lamellipodium, both of which were constantly observed phenotypes. In addition, upon 7 days in culture in the presence of Y-27632 (*e.g.* Fig. 1), we could observe a 30–40% reduction in the number of hematopoietic cells (n = 4, data not shown), which reflect a certain impairment of proliferation. Rho kinase has been shown to be involved in cytokinesis via the phosphorylation of myosin light chain at the cleavage furrow, resulting in its ingression (31). Because the above-referred morphological alterations were also observed after 2 or 3 days of co-culture in the presence of Y-27632, all subsequent experiments were performed within this time range.

Redistribution of Plasma Membrane and Cytoskeleton Proteins upon Inhibition of the ROCK Pathway—The morphological alterations observed in Y-27632-treated cells prompted us to investigate the potential redistribution of classic membrane and cytoskeleton constituents found in plasma membrane protrusions. Untreated (control) and Y-27632-treated HSPCs were immunolabeled for the membrane protein prominin-1 and the cytoskeleton-associated protein ezrin, two proteins concentrated in microvilli and uropods (2, 10, 32). In untreated cells exhibiting a spherical morphology, prominin-1 is often concentrated in one side of the cells (Fig. 2*A*, *curved line*) as previously demonstrated (25). This prominin-1 clustering reflects the formation of a microvillar pole (6, 25). The distribution of ezrin is also polarized (Fig. 2*B*). In cells with an elongated morphology, both proteins are found in the uropod (Fig. 2, *C* and *D*). Interestingly, upon incubation with Y-27632, they are redistributed over either the entire cell surface, in the case of prominin-1 (Fig. 2, *F* and *H*), or cytoplasm, in the case of ezrin (Fig. 2, *G* and *I*). Another uropod-associated protein PSGL-1 behaved similarly (Fig. 2, *E versus J*). Of note, the presence of prominin-1, a hematopoietic stem cell marker, validated the fact that our observations were performed on cells with primitive properties (33).

ROCK Is Required for the Retraction of the Trailing Tail—Do the morphological alterations observed upon inhibition of Rho kinase influence the capacity of HSPCs to migrate? To answer this question, a Transwell assay was performed. The chemotactic factor SDF-1α was added to the lower chamber to stimulate the migration of HSPCs, which were placed in the upper chamber (for technical details see "Experimental Procedures"). After 1-h incubation, we could observe a significant reduction of migrated cells in samples treated with Y-27632 (Fig. 3*A*). Indeed, approximately half of them did not reach the lower compartment (Fig. 3*A*).

To understand how the migration process of these Y-27632-treated cells was affected, time-lapse movies were created. Untreated cells moved by extending a lamellipodium at the leading front (Fig. 3*B*, *Control*, *arrow*) while retracting the uropod at the rear (Fig. 3*B*, *Control*, *outlined arrowhead*). In contrast, Y-27632-treated HSPCs started moving in the direction of the leading protrusion (Fig. 3*B*, *Y-27632*, *arrow*) but demonstrated impairment in retracting the plasma membrane protrusion located at the rear pole (Fig. 3*B*, *Y-27632*, *frame 12′30″*, *white arrowhead*). Moreover, we often observed the formation of a third plasma membrane protrusion (Fig. 3*B*, *Y-27632*, *frame 12′30″*, *black arrowhead*) in agreement with the scanning electron microscopy analysis (Fig. 1*B*) suggesting lack of orientation. In fact, Y-27632-treated HSPCs frequently changed their direction of movement by 180°, converting the tail into the leading edge and vice versa (see supplemental video S2), which indicates that the front-rear orientation is perturbed. A similar feature has been reported in a study performed with monocytes (18).

Finally, by tracking the movement of individual HSPCs (n = 10) for a period of 90 min, we have built a two-dimensional movement diagram. The difference observed between control and Y-27632-treated HSPCs is striking, as the latter cells migrated about half the path that their untreated counterparts did (Fig. 3*B*, *right-side panels*).

ROCK I Activity Is Essential for the Formation of a Uropod and Cell Migration—Given that Y-27632 might inhibit as well the conventional protein kinase C, cAMP-dependent protein kinase, and myosin light-chain kinase, although to a lower extent (34), we used a RNAi-mediated knockdown approach to dissect further and specify the previous results. As there are two mammalian Rho kinase gene products, ROCK I and II, both sensitive to Y-27632 (34), it was of interest to determine separately their ability to regulate morphological and migrational aspects of HSPCs. The design of short interfering RNA (siRNA) oligonucleotides was done in the way that no cross-knockdown was observed (Fig. 4*A*). Overall the knockdown resulted in a reduction of ≈60% ROCK I or II ($n = 3$). Morphologically, the HSPCs transfected with ROCK I siRNA were either spherical (Fig. 4*B*, *outlined arrowhead*) or exhibited long and thin plasma membrane protrusions (Fig. 4*B*, *filled arrowhead*; for quantification see Fig. 4*C*, *middle panel*) as described for Y-27632-treated cells (Fig. 1*B*). Likewise the number of cells exhibiting a uropod was significantly reduced by comparison to the MOCK- or siRNA control-transfected cells (Fig. 4*C*, *upper panel*). Consequently, a reduction in the polarized distribution of ezrin was observed (Fig. 4*C*, *lower panel*). Functionally, the migration of ROCK I siRNA-treated cells was impaired (Fig. 4*D*). Surprisingly, under the same conditions ROCK II siRNA transfectants were morphologically undistinguishable from the control HSPCs (Fig. 4, *B* and *C*) and migrated normally (Fig. 4*D*). The combination of ROCK I and II siRNAs appeared to accentuate the described ROCK I phenotype (Fig. 4, *B* and *D*), although not always statistically significant (Fig. 4*C*). These data suggest that ROCK I has a prevalent role in the morphology of HSPCs and, hence, their locomotion.

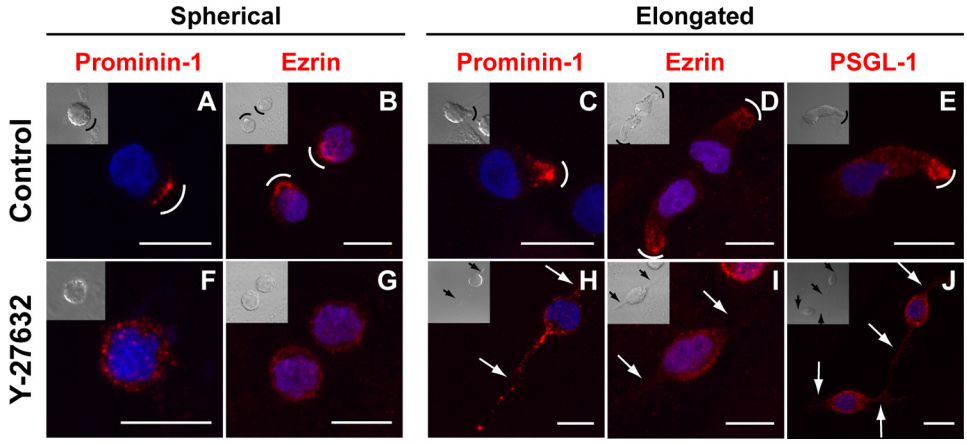

FIGURE 2. **Redistribution of membrane and cytoplasmic proteins upon treatment of hematopoietic progenitors with the ROCK inhibitor Y-27632.** HSPCs cultured on MSCs for 3 days in the absence (*A–E*) or presence (*F–J*) of Y-27632 were analyzed by indirect immunofluorescence either by cell surface labeling (*A*, *C*, *F*, and *H*) or upon permeabilization (*B*, *D*, *E*, *G*, *I*, and *J*). HSPCs exhibiting either a spherical (*A*, *B*, *F*, and *G*) or elongated (*C–E* and *H–J*) morphology are depicted. *A–E*, the distribution of prominin-1, ezrin and PSGL-1 (all in *red*) is polarized in untreated HSPCs (*A* and *C*, prominin-1; *B* and *D*, ezrin; and *E*, PSGL-1). *F–J*, in the presence of Y-27632, prominin-1 (*F* and *H*), ezrin (*G* and *I*), and PSGL-1 (*J*) are redistributed over the entire plasma membrane or cytoplasm. A differential interference contrast image is shown in the *inset*. Nuclei were visualized with DAPI (*blue*). *Curved lines* indicate the clustering of either prominin-1, ezrin, or PSGL-1; *arrows* point to the long and thin plasma membrane protrusions observed in Y-27632-treated cells. *Scale bars*, 10 μm.

The Tubulin Network Is Actively Involved in Cell Migration—We then sought for the cytoskeleton elements that, upon Y-27632-induced inhibition of ROCK, could be responsible for the defective retrac-

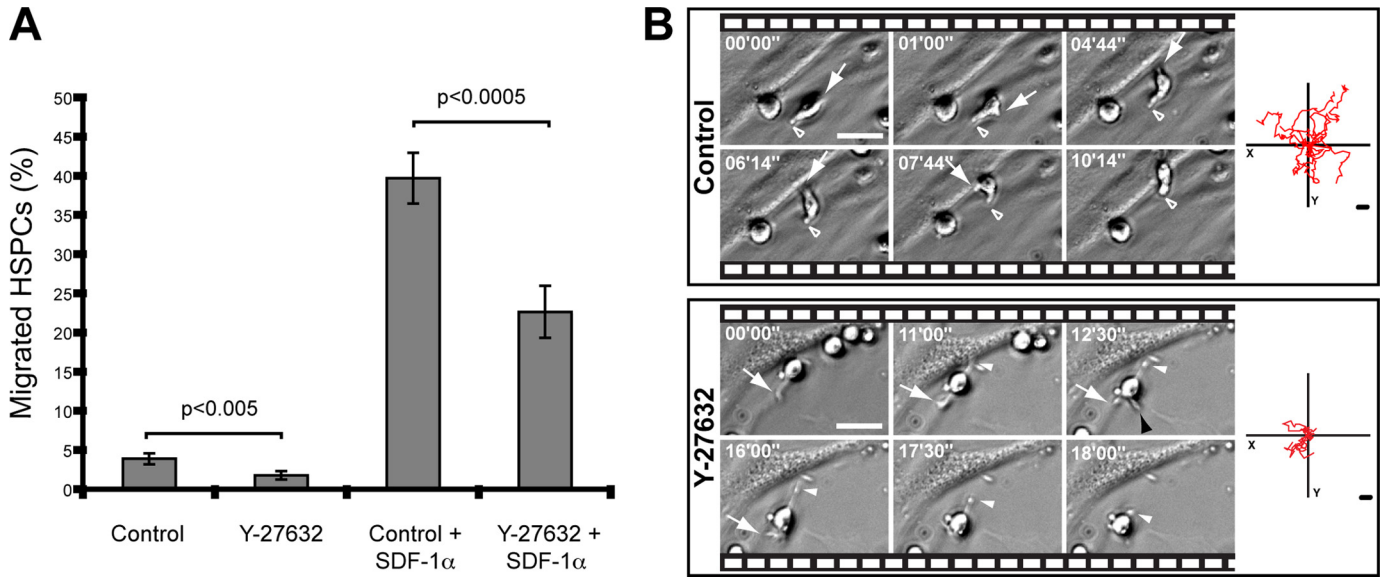

FIGURE 3. **ROCK inhibitor Y-27632 alters the migration of hematopoietic progenitors.** *A*, Transwell assay of untreated (*Control*) or Y-27632-treated HSPCs in the absence or presence of SDF-1α. The number of hematopoietic cells that migrated from the upper to the lower chamber after 1-h incubation is plotted as a percentage of total cells loaded (12.5×10^4). Statistical analysis: *t* test. *B*, time-lapse video analysis of the migration of HSPCs. The *arrow* indicates the migrating front, whereas the *outlined* and *filled white arrowheads* point to the rear pole of HSPC present in the control or Y-27632-treated sample, respectively; the *black arrowhead* shows a third plasma membrane protrusion growing out from an Y-27632-treated HSPC. The elapsed time is shown in the *upper left corner* of each frame. *Diagrams* in the *right panel* depict the movement of 10 individual HSPCs for a period of 90 min. *Scale bars*, 15 μm.

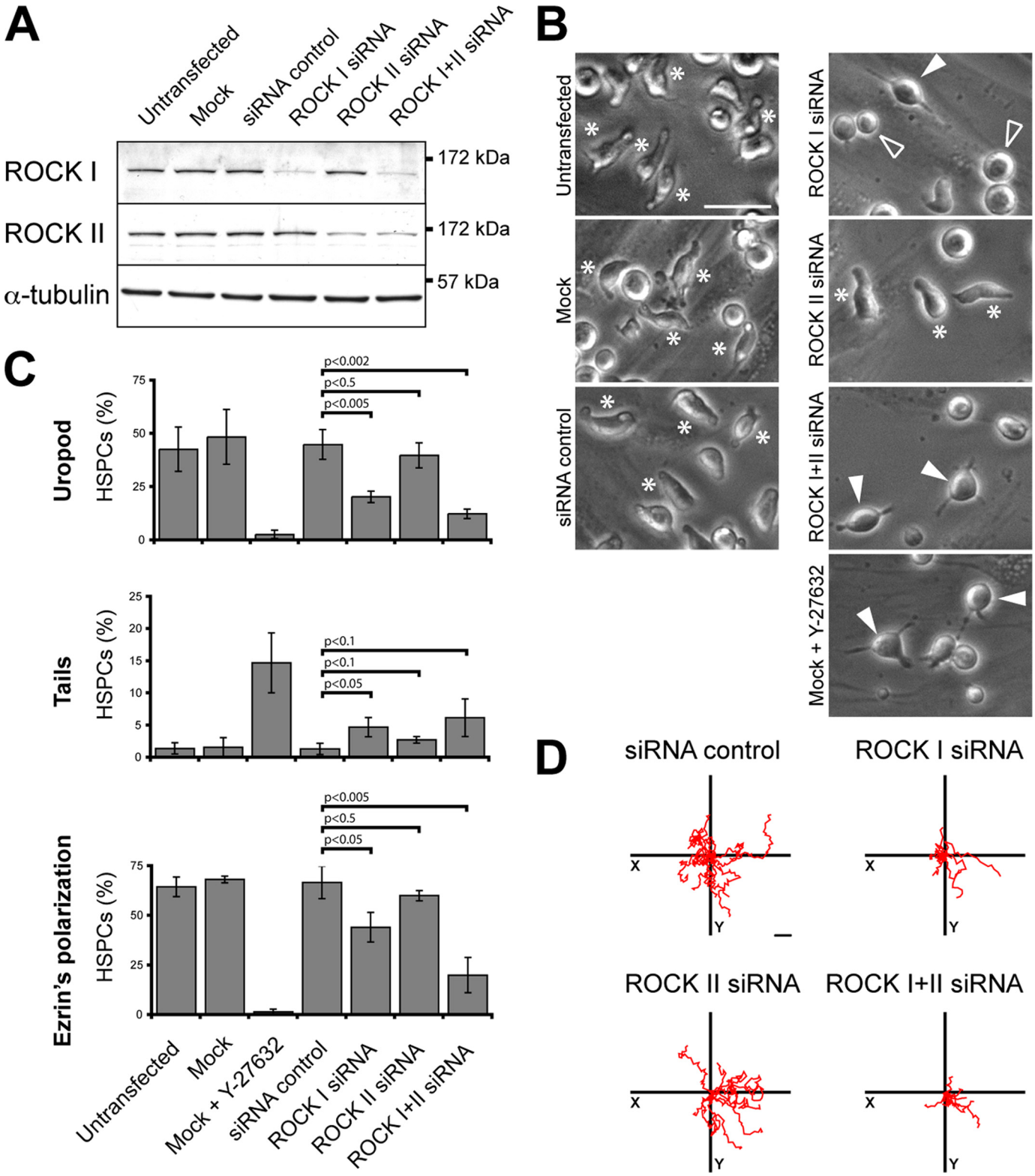

FIGURE 4. **ROCK I, but not ROCK II, is essential for the polarization and migration of hematopoietic progenitors.** *A–D*, HSPCs were either untransfected or transfected with the indicated siRNA or without (*Mock*) prior to cultivation on MSCs for 2 days. *A*, ROCK I and II knockdowns were confirmed by immunoblotting of the total proteins extracted from the different transfectants. α-Tubulin was used as a control for the protein loading. *B*, HSPC morphology was analyzed by bright field microscopy. *Asterisks* indicate HSPCs with a uropod; *filled arrowheads* indicate HSPCs bearing long and thin plasma membrane protrusions; *outlined arrowheads* point cells with a spherical morphology. *C*, quantitative analysis of the HSPCs harboring either a uropod (*upper panel*) or a long plasma membrane protrusion as a trailing tail (*middle panel*) in the different transfectants. The polarization of ezrin (evaluated by fluorescence microscopy) in different transfectants is shown in the *lower panel*. The data are expressed as percentage of total HSPCs (200 cells were counted per condition; $n = 3$). Statistical analysis: *t* test. *D*, tracking diagrams based on time-lapse videos depict the movement of ten individual HSPCs for a period of 50 min. *Scale bars*, 20 μm.

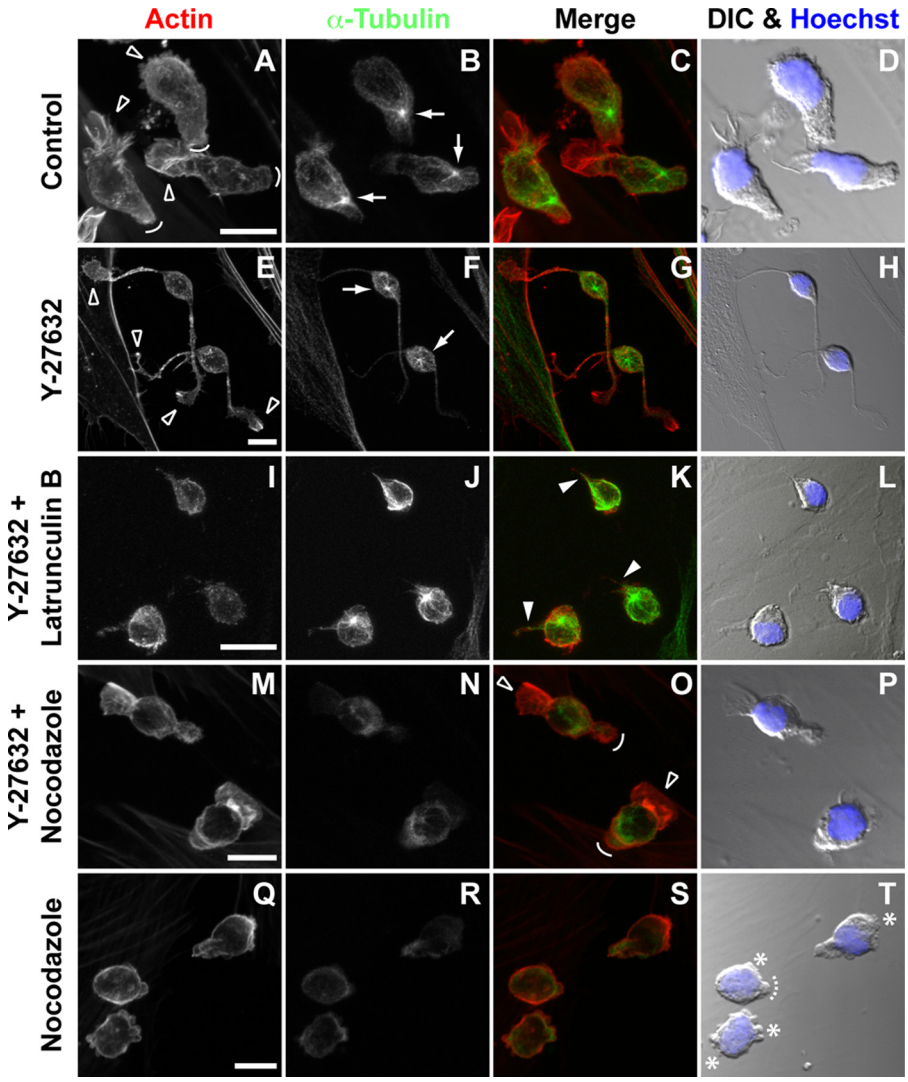

FIGURE 5. **The microtubule network is involved in the tail retraction of migrating hematopoietic progenitors.** *A–T*, HSPCs cultured on MSCs were subjected to different treatments as indicated, prior to actin (*red*) and α-tubulin (*green*) fluorescence labeling and confocal microscopy analysis. Composites of 7–10 *x-z* optical sections are shown. Nuclei were visualized by Hoechst labeling (*blue*). Differential interference contrast (*DIC*) images are shown (*D*, *H*, *L*, *P*, and *T*). *A–D*, untreated HSPCs (*Control*); *outlined arrowheads* point the lamellipodium (migrating front), whereas *curved lines* indicate the uropod (rear pole of migrating cells). *Arrows* show the position of the centrosome. *E–H*, Y-27632-treated HSPCs; *outlined arrowheads* indicate lamellipodia at the edge of the long and thin plasma membrane protrusions induced by Y-27632 treatment, and *arrows* show the position of the centrosome. *I–L*, depolymerization of actin filaments with latrunculin B in Y-27632-treated HSPCs; *filled arrowheads* indicate reminiscent tails. *M–P*, depolymerization of microtubules with nocodazole in Y-27632-treated HSPCs; *outlined arrowheads* and *curved lines* indicate the restored lamellipodium and the uropod-like structure, respectively. *Q–T*, depolymerization of microtubules with nocodazole in HSPCs; *asterisks* indicate bleb-like membrane protrusions, whereas the *dashed curved line* shows a remnant of a uropod. *Scale bars*, 10 μm.

tion of the thin and long plasma membrane protrusion located at the rear pole. To investigate this issue we selectively induced the depolymerization of either actin filaments or the tubulin network. In untreated cells, actin filaments were enriched in the lamellipodium at the leading edge (Fig. 5, *A* and *C*, *outlined arrowheads*), whereas tubulin highlighted the centrosome located in a zone between the nucleus and the uropod (Fig. 5, *B* and *C*, *arrows*). The asymmetric distribution of the centrosome was lost upon Y-27632-treatment (Fig. 5, *F* and *G*, *arrows*) and actin became randomly distributed (Fig. 5, *E* and *G*). In the presence of Y-27632, the actin depolymerization triggered by latrunculin B resulted in cells that, as expected, completely lost the lamellipodium but nonetheless still exhibited a short unretracted tail (Fig. 5, *I–L*, *filled arrowheads*). Remarkably, the depolymerization of microtubules triggered by nocodazole led to the effective retraction of the Y-27632-induced plasma membrane protrusions resulting in both (i) the formation of a structure that presented a striking similarity to a uropod (Fig. 5*O*, *curved line*) and (ii) the restoration of the lamellipodium-uropod axis (Fig. 5*O*, *outlined arrowhead* and *curved line*, respectively). In contrast, the nocodazole treatment alone resulted in numerous membrane blebs (Fig. 5, *Q–T*, *asterisks*; see supplemental video S3), which is in line with an early report (35). Furthermore, although small uropod-like structures were often observed (Fig. 5*T*, *dashed curved line*) the general cell polarity, *i.e.* lamellipodium-uropod axis, was altered.

At the molecular level, prominin-1, PSGL-1, and ezrin redistributed into the nocodazole-induced uropod of Y-27632-treated cells (Fig. 6*A*) as observed in the untreated samples (Fig. 2) indicating that certain membrane and cytoskeleton constituents are correctly positioned, which is not necessarily the case in cells incubated with nocodazole alone (supplemental Fig. S2).

Does the nocodazole treatment also rescue the phenotype observed upon ROCK I siRNA-mediated knockdown? Indeed, the percentage of HSPCs displaying a uropod dramatically increased upon addition of nocodazole to the ROCK I siRNA transfectants (Fig. 6*B*). The same phenomenon is observed for the double ROCK I + II siRNA transfectants (Fig. 6*B*). Besides recovering the uropod, the depolymerization of microtubules restores the migration of HSPCs (Fig. 6*C*; see supplemental video S4), suggesting that microtubules are directly involved in the deficiency of rear retraction caused by the inhibition or knockdown of ROCK I.

Implication of RhoA in Cell Migration—To get more insight into the Rho-kinase upstream determinants, we knocked down the expression of RhoA using siRNA technology. Under these conditions, the expression of RhoA was decreased by >90% (Fig. 7*A*, $n = 3$). The morphology of the RhoA siRNA-transfected HSPCs is similar to those treated with Y-27632 (Fig. 7*B*; for comparison see Fig. 1*B*). A significant decrease in cells

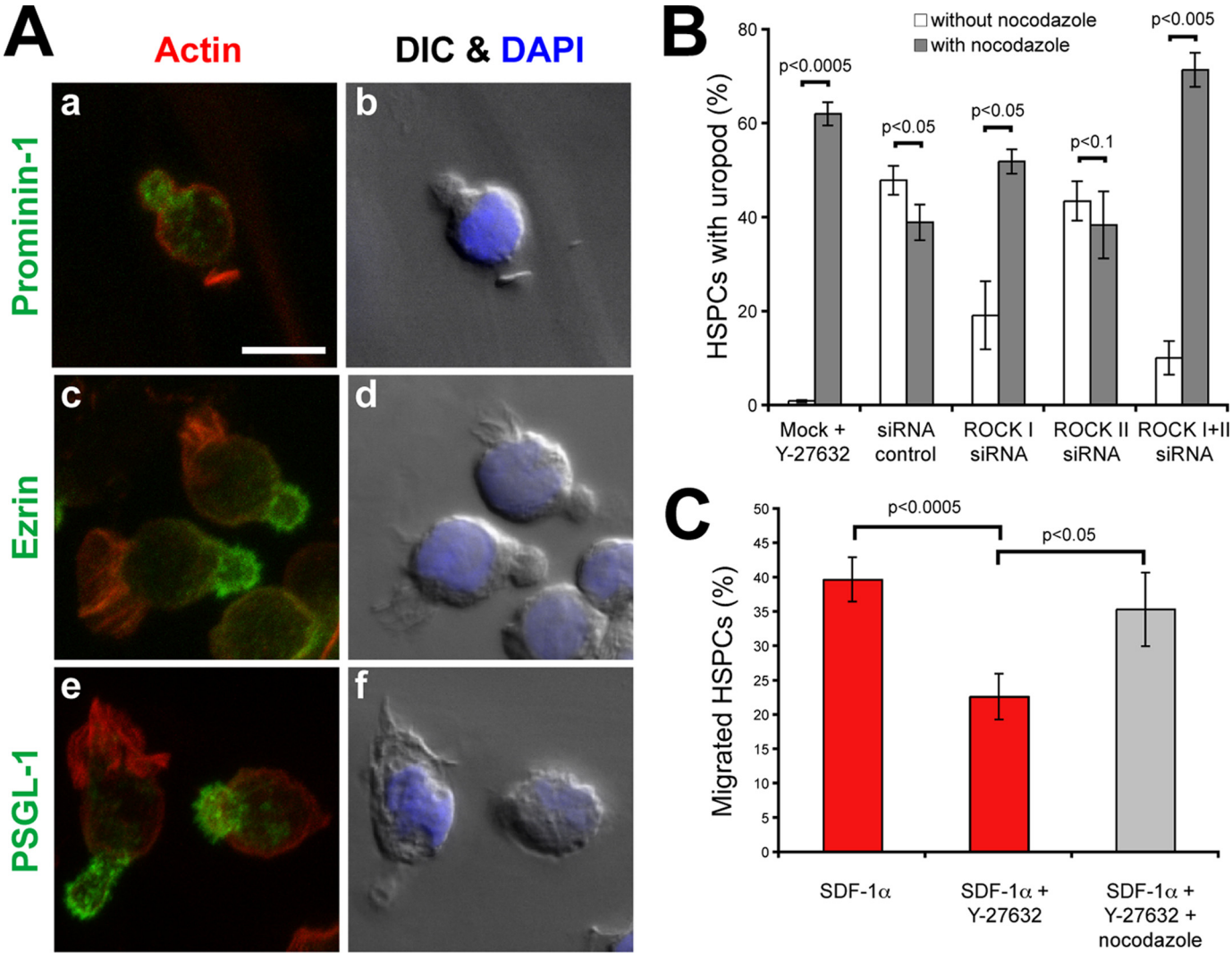

FIGURE 6. **Microtubule depolymerization restores the polarization and migration of Y-27632-treated hematopoietic progenitors.** *A*, nocodazole/Y-27632-treated HSPCs cultured on MSCs for 3 days were analyzed by indirect immunofluorescence upon permeabilization for prominin-1 (*a*, *green*), ezrin (*c*, *green*), and PSGL-1 (*e*, *green*). Actin (*a*, *c*, and *e*; *red*) and nuclei (*b*, *d*, and *f*; *blue*) were visualized with Phalloidin and DAPI labeling, respectively. Differential interference contrast (*DIC*) images are shown (*b*, *d*, and *f*). *Scale bar*, 10 μm. *B*, depolymerization of microtubules with nocodazole restores the uropod formation in ROCK I and ROCK I + II siRNA-transfected HSPCs. Number of uropods was determined via phase-contrast microscopy (200 cells were counted per condition; $n = 3$). Note that in the nocodazole-treated siRNA control and ROCK II siRNA samples only a remnant of uropod was observed (see also Fig. 5*T*). *C*, Transwell assay of nocodazole/Y-27632-treated HSPCs in the presence of SDF-1α. Number of hematopoietic progenitors that migrated from the upper to the lower chamber after 1 h is plotted as a percentage of total cells loaded (12.5×10^4). (For comparison purposes, data shown in Fig. 3*A* are indicated in *red*, because all data were acquired in parallel.) Statistical analysis in *B* and *C*: *t* test.

harboring a uropod and an increase in cells with thin and long plasma membrane protrusions was observed (Fig. 7*C*, *upper* and *middle panels*, respectively). As a consequence, ezrin lost its polarized distribution (Fig. 7*C*, *lower panel*). Functionally, the down-regulation of RhoA impaired the capacity of HSPCs to migrate (Fig. 7*D*).

DISCUSSION

Stem cells are characterized by their potential to self-renew and differentiate upon encountering the appropriate cues. Another important characteristic of these rare cells is their strong ability to migrate. Here we have dissected the latter feature at the cellular and molecular levels and report two important findings. First, we demonstrated that the formation and/or maintenance of a uropod at the rear pole of a migrating HSPC is dependent on RhoA and its downstream effector ROCK I. Second, an active reorganization of the microtubule network, which is dependent of RhoA/ROCK activity, is essential for their proper migration.

Thus three plasma membrane-protruding structures of HSPCs appear controlled, at least in part, by the RhoA/ROCK pathway: microvillar-like structures, lamellipodium, and uropod. The ablation of the latter upon either inhibition or knockdown of RhoA or ROCK I, which is followed by the formation of a trailing tail and a redistribution of membrane (prominin-1 and PSGL-1) and cytoskeleton (ezrin) proteins, leads to the impairment of cell migration. These observations are consistent with early reports showing that Rho kinase inhibitor Y-27632 induces a long tail that remains behind the cells (*e.g.* T cells) because of posterior retraction defects (36, 37). Remarkably, both morphologically and functionally, these alterations could be rescued by depolymerizing microtubules with nocoda-

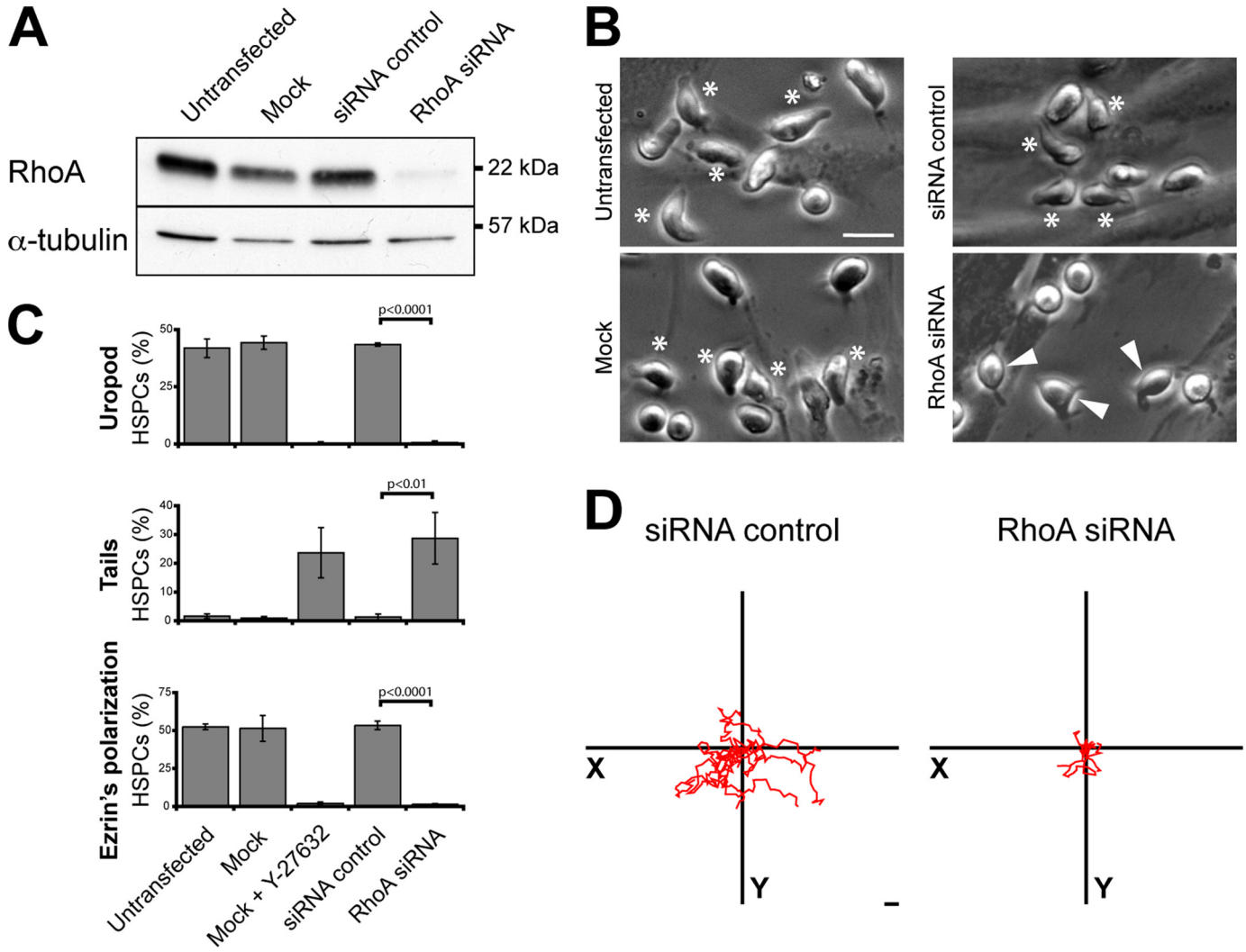

FIGURE 7. **RhoA controls the polarization and migration of hematopoietic progenitors.** *A–D*, HSPCs were either untransfected or transfected with the indicated siRNA or without (*Mock*) prior to cultivation on MSCs. *A*, RhoA knockdown was confirmed by immunoblotting of the total protein extracted from the different transfectants. α-Tubulin was used as a control for the protein loading. *B*, HSPC morphology was analyzed by bright field microscopy. *Asterisks* and *filled arrowheads* indicate HSPCs bearing either a uropod or long and thin plasma membrane protrusions, respectively. *C*, quantitative analysis of the HSPCs harboring either a uropod (*upper panel*) or a long plasma membrane protrusion as a trailing tail (*middle panel*) in the different transfectants. The polarization of ezrin (evaluated by fluorescence microscopy) in different transfectants is shown in the *lower panel*. The data are expressed as the percentage of total HSPCs (200 cells were counted per condition; $n = 3$). Statistical analysis: *t* test. *D*, tracking diagrams based on time-lapse videos depict the movement of 10 individual HSPCs for a period of 50 min. *Scale bars*, 20 μm.

zole indicating a relationship between the RhoA/ROCK pathway and the microtubule network. Specifically, the activity of RhoA, and notably ROCK I but not ROCK II, appears essential to destabilize the microtubule structure at the rear pole of migrating HSPCs, and hence to promote their locomotion (for a model, see supplemental Fig. S3). The physiological role of ROCK II in HSPCs remains to be elucidated. Nevertheless, by analogy to keratinocytes, this second Rho kinase might be involved in the terminal differentiation of HSPCs (38).

The particular way Rho kinase signals to the microtubule network remains to be determined. Previous studies have demonstrated that, in other cell types, Rho GTPases regulate (or are regulated) by microtubule dynamics. For instance, nocodazole-induced microtubule disassembly releases a microtubule-associated GEF (GEF-H1), which activates RhoA, suggesting that many of the effects solely attributed to microtubules are actually caused by the activation of RhoA (39–41). In the case of the HSPCs, this mechanism did not appear to play a predominant role, because no overactivation of RhoA upon nocodazole-induced microtubule depolymerization was observed using a Rho-binding domain pull-down assay.[4] However, such GEF-dependent activation of RhoA will not restore the proper cell locomotion, because ROCK activity remains perturbed, unless an alternative unidentified pathway is involved (supplemental Fig. S3).

As recently discussed by Takesono and colleagues, who have observed a similar feedback loop between the Rho/ROCK signaling pathway and microtubule dynamics in an acute T lymphoblastic leukemia cell line (42), many downstream (direct or indirect) targets such as myosin II and/or enzymes that mediate tubulin acetylation and detyrosination might be involved (43,

[4] A.-V. Fonseca and D. Corbeil, unpublished data.

44). Likewise microtubule-destabilizing protein stathmin/OP18 might also participate in these biochemical reactions (45), and both the partial alteration of the lamellipodium and the perturbation of the front-rear orientation observed in Y-27632-treated HSPCs are coherent with it. Moreover, in the absence of RhoA/ROCK pathway, Rac (and Cdc42) might participate in the maintenance of the lamellipodium (although altered) by inhibiting the actin-depolymerizing activity of cofilin throughout p21-activated kinase and LIM kinases (46). The constitutive secretion of SDF-1, an activator of Rac (47), by feeder cells might be relevant in this context (25). Furthermore, ROCK has been shown to phosphorylate and hence activate FilGAP (a filamin A-binding RhoGTPase-activating protein), leading to the inactivation of Rac (48). Thus, in the absence of functional ROCKs, the activity of Rac is not switched off by FilGAP, which would sustain the imbalanced leading-lamellae activity of Y-27632-treated HSPCs.

In addition to these complex interplays, we could not ignore a potential role of cholesterol-based membrane microdomains. In HSPCs, both the lamellipodium and the uropod are enriched with specific membrane microdomains containing either gangliosides GM3 or GM1 (named according to Svennerholm's nomenclature), respectively (2, 6, 9). The integrity of these structures might be regulated not only by lipids (cholesterol and ganglioside) (9) but also by certain proteins found therein. In agreement with this idea, we could observe a redistribution of certain membrane components, including prominin-1, a lipid raft-associated protein (49), in Y-27632-treated HSPCs. The membrane microdomain-resident integral proteins might be linked to the actin-cytoskeleton via ERM proteins, *i.e.* potential targets of Rho kinase (50, 51) (supplemental Fig. S3). Indeed, the adaptor protein ezrin has been previously demonstrated to play an active role in membrane microdomain dynamics (52). It remains to be established whether ERM proteins are phosphorylated directly by ROCK I, a process that has been shown to be dependent either on the cell types or culture conditions (53). Nevertheless the redistribution of ezrin (like prominin-1) in Y-27632-treated HSPCs harboring either spherical or elongated morphology suggests a potential link. Also, ERM proteins are involved in the integrity of the microvilli and/or microvillar-like structures (54). It might be more than a coincidence that, in addition to the redistribution of ezrin, microvillar projections are disrupted upon the incubation of cells with Y-27632. However, other ERM proteins might regulate the formation and/or stabilization of microvillar-like projections such as moesin (55). Naturally, further dissection of putative player(s) is urged.

Physiologically, an elegant study using murine HSPCs infected with a dominant-negative mutant of RhoA (RhoAN19) has shown that, *in vitro*, these cells display reduced migration toward SDF-1 and adhesion compared with control cells (56), as we have demonstrated here for their human counterparts. However, the reduced RhoA activity was associated with a higher proliferation rate *in vivo*, which results in a net increase of engraftment within the bone marrow microenvironment (56). Although the authors did not observe obvious effects on cell differentiation (56), the latter phenomenon might be related to ROCK II (see above). Thus a fine-tuning balance between cell migration and proliferation/self-renewal capacity appears essential for the success of transplantation.

In conclusion, our data support a model where the activity of RhoA and its effector ROCK I contributes to plasma membrane polarization, and hence migration, of HSPCs. In essence, our co-culture system and the effective RNAi-based down-regulation of specific targets may help us identify additional players in these complex processes. Those highlighted in the present study may represent potential targets to develop strategies that could improve the rate of engraftment, especially in cases where the amount of available HSPCs is restricted, as those derived from the cord blood.

Acknowledgments—We thank Prof. Dr. Carsten Werner for the use of the scanning electron microscope, and members of the Corbeil laboratory for discussion and support.

REFERENCES

1. Wright, D. E., Wagers, A. J., Gulati, A. P., Johnson, F. L., and Weissman, I. L. (2001) *Science* **294,** 1933–1936
2. Giebel, B., Corbeil, D., Beckmann, J., Höhn, J., Freund, D., Giesen, K., Fischer, J., Kögler, G., and Wernet, P. (2004) *Blood* **104,** 2332–2338
3. Barreiro, O., de la Fuente, H., Mittelbrunn, M., and Sánchez-Madrid, F. (2007) *Immunol. Rev.* **218,** 147–164
4. del Pozo, M. A., Cabañas, C., Montoya, M. C., Ager, A., Sánchez-Mateos, P., and Sánchez-Madrid, F. (1997) *J. Cell Biol.* **137,** 493–508
5. Friedl, P., Entschladen, F., Conrad, C., Niggemann, B., and Zänker, K. S. (1998) *Eur. J. Immunol.* **28,** 2331–2343
6. Bauer, N., Fonseca, A. V., Florek, M., Freund, D., Jaszai, J., Bornhäuser, M., Fargeas, C. A., and Corbeil, D. (2008) *Cells Tiss. Org.* **188,** 127–138
7. Sánchez-Madrid, F., and del Pozo, M. A. (1999) *EMBO J.* **18,** 501–511
8. Giebel, B., and Beckmann, J. (2007) *Cell Cycle* **6,** 2201–2204
9. Gillette, J. M., Larochelle, A., Dunbar, C. E., and Lippincott-Schwartz, J. (2009) *Nat Cell Biol.* **11,** 303–311
10. Lee, J. H., Katakai, T., Hara, T., Gonda, H., Sugai, M., and Shimizu, A. (2004) *J. Cell Biol.* **167,** 327–337
11. Sánchez-Madrid, F., and Serrador, J. M. (2009) *Nat. Rev. Mol. Cell Biol.* **10,** 353–359
12. Etienne-Manneville, S., and Hall, A. (2002) *Nature* **420,** 629–635
13. Ridley, A. J., and Hall, A. (1992) *Cell* **70,** 389–399
14. Nobes, C. D., and Hall, A. (1995) *Cell* **81,** 53–62
15. Ridley, A. J., Paterson, H. F., Johnston, C. L., Diekmann, D., and Hall, A. (1992) *Cell* **70,** 401–410
16. O'Connor, K. L., Nguyen, B. K., and Mercurio, A. M. (2000) *J. Cell Biol.* **148,** 253–258
17. Kurokawa, K., and Matsuda, M. (2005) *Mol. Biol. Cell* **16,** 4294–4303
18. Worthylake, R. A., Lemoine, S., Watson, J. M., and Burridge, K. (2001) *J. Cell Biol.* **154,** 147–160
19. Alblas, J., Ulfman, L., Hordijk, P., and Koenderman, L. (2001) *Mol. Biol. Cell* **12,** 2137–2145
20. Ishizaki, T., Maekawa, M., Fujisawa, K., Okawa, K., Iwamatsu, A., Fujita, A., Watanabe, N., Saito, Y., Kakizuka, A., Morii, N., and Narumiya, S. (1996) *EMBO J.* **15,** 1885–1893
21. Leung, T., Chen, X. Q., Manser, E., and Lim, L. (1996) *Mol. Cell. Biol.* **16,** 5313–5327
22. Matsui, T., Amano, M., Yamamoto, T., Chihara, K., Nakafuku, M., Ito, M., Nakano, T., Okawa, K., Iwamatsu, A., and Kaibuchi, K. (1996) *EMBO J.* **15,** 2208–2216
23. Nakagawa, O., Fujisawa, K., Ishizaki, T., Saito, Y., Nakao, K., and Narumiya, S. (1996) *FEBS Lett.* **392,** 189–193
24. Yoneda, A., Multhaupt, H. A., and Couchman, J. R. (2005) *J. Cell Biol.* **170,** 443–453
25. Freund, D., Bauer, N., Boxberger, S., Feldmann, S., Streller, U., Ehninger, G., Werner, C., Bornhäuser, M., Oswald, J., and Corbeil, D. (2006) *Stem.*

Cells Dev. **15,** 815–829
26. von Levetzow, G., Spanholtz, J., Beckmann, J., Fischer, J., Kögler, G., Wernet, P., Punzel, M., and Giebel, B. (2006) *Stem. Cells Dev.* **15,** 278–285
27. Majumdar, M. K., Thiede, M. A., Mosca, J. D., Moorman, M., and Gerson, S. L. (1998) *J. Cell. Physiol.* **176,** 57–66
28. Freund, D., Fonseca, A. V., Janich, P., Bornhäuser, M., and Corbeil, D. (2010) *Cytotherapy* **12,** 131–142
29. Corbeil, D., Röper, K., Hannah, M. J., Hellwig, A., and Huttner, W. B. (1999) *J. Cell Sci.* **112,** 1023–1033
30. Corbeil, D., Fargeas, C. A., and Huttner, W. B. (2001) *Biochem. Biophys. Res. Commun.* **285,** 939–944
31. Kosako, H., Yoshida, T., Matsumura, F., Ishizaki, T., Narumiya, S., and Inagaki, M. (2000) *Oncogene.* **19,** 6059–6064
32. Weigmann, A., Corbeil, D., Hellwig, A., and Huttner, W. B. (1997) *Proc. Natl. Acad. Sci. U.S.A.* **94,** 12425–12430
33. Miraglia, S., Godfrey, W., Yin, A. H., Atkins, K., Warnke, R., Holden, J. T., Bray, R. A., Waller, E. K., and Buck, D. W. (1997) *Blood* **90,** 5013–5021
34. Uehata, M., Ishizaki, T., Satoh, H., Ono, T., Kawahara, T., Morishita, T., Tamakawa, H., Yamagami, K., Inui, J., Maekawa, M., and Narumiya, S. (1997) *Nature* **389,** 990–994
35. Jia, Z., Vadnais, J., Lu, M. L., Noël, J., and Nabi, I. R. (2006) *Biol. Cell* **98,** 337–351
36. Worthylake, R. A., and Burridge, K. (2001) *Curr. Opin. Cell Biol.* **13,** 569–577
37. Smith, A., Bracke, M., Leitinger, B., Porter, J. C., and Hogg, N. (2003) *J. Cell Sci.* **116,** 3123–3133
38. Lock, F. E., and Hotchin, N. A. (2009) *Plos. One.* **4,** e8190
39. Enomoto, T. (1996) *Cell Struct. Funct.* **21,** 317–326
40. Krendel, M., Zenke, F. T., and Bokoch, G. M. (2002) *Nat. Cell Biol.* **4,** 294–301
41. Chang, Y. C., Nalbant, P., Birkenfeld, J., Chang, Z. F., and Bokoch, G. M. (2008) *Mol. Biol. Cell* **19,** 2147–2153
42. Takesono, A., Heasman, S. J., Wojciak-Stothard, B., Garg, R., and Ridley, A. J. (2010) *Plos. One* **5,** e8774
43. Eddy, R. J., Pierini, L. M., Matsumura, F., and Maxfield, F. R. (2000) *J. Cell Sci.* **113,** 1287–1298
44. Xu, J., Wang, F., Van Keymeulen, A., Herzmark, P., Straight, A., Kelly, K., Takuwa, Y., Sugimoto, N., Mitchison, T., and Bourne, H. R. (2003) *Cell* **114,** 201–214
45. Marklund, U., Larsson, N., Gradin, H. M., Brattsand, G., and Gullberg, M. (1996) *EMBO J.* **15,** 5290–5298
46. Riento, K., and Ridley, A. J. (2003) *Nat. Rev. Mol. Cell Biol.* **4,** 446–456
47. Nijhara, R., van Hennik, P. B., Gignac, M. L., Kruhlak, M. J., Hordijk, P. L., Delon, J., and Shaw, S. (2004) *J. Immunol.* **173,** 4985–4993
48. Ohta, Y., Hartwig, J. H., and Stossel, T. P. (2006) *Nat. Cell Biol.* **8,** 803–814
49. Röper, K., Corbeil, D., and Huttner, W. B. (2000) *Nat. Cell Biol.* **2,** 582–592
50. Tran Quang, C., Gautreau, A., Arpin, M., and Treisman, R. (2000) *EMBO J.* **19,** 4565–4576
51. Yoshinaga-Ohara, N., Takahashi, A., Uchiyama, T., and Sasada, M. (2002) *Exp. Cell Res.* **278,** 112–122
52. Gupta, N., Wollscheid, B., Watts, J. D., Scheer, B., Aebersold, R., and DeFranco, A. L. (2006) *Nat. Immunol.* **7,** 625–633
53. Yonemura, S., Matsui, T., Tsukita, S., and Tsukita, S. (2002) *J. Cell Sci.* **115,** 2569–2580
54. Gautreau, A., Louvard, D., and Arpin, M. (2000) *J. Cell Biol.* **150,** 193–203
55. Oshiro, N., Fukata, Y., and Kaibuchi, K. (1998) *J. Biol. Chem.* **273,** 34663–34666
56. Ghiaur, G., Lee, A., Bailey, J., Cancelas, J. A., Zheng, Y., and Williams, D. A. (2006) *Blood* **108,** 2087–2094